

Search for possible neutrino radiative decays during the 2001 total solar eclipse

S. Cecchini ^{a,b} D. Centomo ^a G. Giacomelli ^a R. Giacomelli ^a
V. Popa ^{a,c} C.G. Șerbănuț ^{a,c} R. Serra ^{a,d}

^a*Dipartimento di Fisica dell'Università and INFN Sezione di Bologna, I-40127
Bologna, Italy*

^b*IASF/CNR, I-40129 Bologna, Italy*

^c*Institute for Space Sciences, R-77125 Bucharest Măgurele, Romania*

^d*Osservatorio Astronomico, I-40017 San Giovanni in Persiceto, Italy*

Abstract

We present the results of the observations performed in the occasion of the June 21st, 2001 total solar eclipse, looking for visible photons emitted through a possible radiative decay of solar neutrinos. We establish lower limits for the ν_2 or ν_3 proper lifetimes $\tau_0/m \geq 10^3$ s/eV, for neutrino masses larger than 10^{-2} eV.

Key words: Solar neutrinos, Decays of heavy neutrinos, Neutrino mass and mixing, Total solar eclipses, Image processing

PACS: 96.60.Vg, 13.35.Hb, 14.60.Pq, 95.85.Ry, 95.75.Mn

1 Introduction

In the last few years it has become clear that neutrinos have non-vanishing masses, and that the neutrino flavor eigenstates (ν_e , ν_μ and ν_τ) are superpositions of mass eigenstates (ν_1 , ν_2 and ν_3), giving rise to neutrino oscillations. For recent reviews, see [1,2]. In this context, neutrinos can undergo radiative decays, e.g. $\nu_2 \rightarrow \nu_1 + \gamma$, as initially suggested in [3]; the first searches for such decays were based on astrophysical considerations (see eg. [4]). The status of the decaying theory and phenomenology was summarized in [5].

Radiative decays are allowed if the involved neutrinos have a non-vanishing magnetic dipole moment; the very stringent existing experimental limits ($\mu_\nu < 1.3 \times 10^{-10} \mu_B$ [6]) refer to the neutrino flavor eigenstates and are not directly applicable to possible dipole magnetic moments of neutrino mass eigenstates.

Neutrino decays (radiative or not) have been searched for indirectly (from astrophysical arguments such as Supernova physics or the absence of γ rays in the Sun radiation, or from IR background measurements), by re-interpreting solar and atmospheric neutrino data from large experiments, as well as directly (experiments near nuclear reactors, analysis with cosmic ray detectors or during total solar eclipses). All published searches yield lower limits for the neutrino lifetimes, which are strongly sensitive to the assumed neutrino mass and mass hierarchy scenario.

The astrophysical neutrino lifetime lower limits are usually large (e.g. $\tau_0/m > 2.8 \times 10^{15} \text{ s eV}^{-1}$ where τ_0 is the lower proper lifetime limit for a neutrino of mass m , [7]), but they are indirect and rather speculative limits.

Much lower “semi-indirect” limits were deduced from the re-interpretation of solar and atmospheric neutrino data. Earlier attempts to explain the solar neutrino or atmospheric neutrino anomalies only in terms of neutrino decay have been ruled out by the existing evidence [8]; the present accepted explanations are based on neutrino oscillations, but do not exclude the hypothesis of neutrino decays. As an example, from the SNO data [9,10] a proper lower limit of $\tau_0/m > 8.7 \times 10^{-5} \text{ s eV}^{-1}$ was deduced [11]. By analyzing all available solar neutrino data, stronger limits were obtained [12]: $\tau_0/m > 22.7 \text{ s MeV}^{-1}$ for the MSW solution, and $\tau_0/m > 27.8 \text{ s MeV}^{-1}$ for the vacuum oscillation solution of the solar neutrino problem (SNP).

Direct searches for radiative neutrino decays have been also performed. As an example we quote here the search for decay photons in the visible spectrum performed in the vicinity of a nuclear reactor [13], yielding τ_0/m lower limits in the range 10^{-8} to nearly 0.1 s eV^{-1} , assuming neutrino relative mass differences $\Delta m/m$ between 10^{-7} and 0.1 . Recently, a search for γ photons, using the Prototype Borexino Detector at Gran Sasso [14] reported τ_0/m lower limits of $1.5 \times 10^3 \text{ s eV}^{-1}$ (assuming a polarization parameter $\alpha = -1$ for the parent neutrino), $4.4 \times 10^3 \text{ s eV}^{-1}$ (for $\alpha = 0$) and $9.7 \times 10^3 \text{ s eV}^{-1}$ (for $\alpha = +1$).

In a pioneering experiment performed during the Total Solar Eclipse (TSE) of October 24, 1995 a search was made for visible photons emitted through radiative decays of solar neutrinos during their flight between the Moon and the Earth [15]. In their analysis, the authors assumed that all neutrinos have masses of the order of few eV, $\Delta m_{12}^2 = m_2^2 - m_1^2 \simeq 10^{-5} \text{ eV}^2$, and an average energy of 860 keV. Furthermore they assumed that all decays would lead to visible photons, which would travel nearly in the same direction as the parent neutrinos, thus leading to a narrow spot of light coming from the direction of the center of the dark disk of the Moon. In the absence of a positive signal, this search yielded a lower proper lifetime of 97 s, for neutrinos with m_ν few eV [15].

Some of the authors of this paper were involved in two similar experiments, during the total solar eclipses of August 11, 1999 (in Romania) [16,17], and of June 21, 2001 (in Zambia) [18,19].

In 1999 the bad weather conditions did not allow the planned observations with the properly designed experimental apparatus; but we could analyse the images of a videotape recorded by a local Romanian television (Râmnicu Vâlcea). The study of the data was performed in the hypothesis of a possible decay

$$\nu_2 \rightarrow \nu_1 + \gamma, \tag{1}$$

with $m_2 > m_1$, and for two values of Δm^2 suggested by the MSW SMA (Small Mixing Angle) and LMA (Large Mixing Angle) solutions of the SNP, allowed by the then available data from solar neutrino experiments.

We developed a Monte Carlo (MC) simulation of radiative solar neutrino decays, considering the neutrino energy spectrum predicted by the Standard Solar Model (SSM) [20] and the mass of the ν_1 in the range of 1 - 10 eV, as it was expected at that time. Since the angular resolution of the data was not very good, we considered the Sun as a pointlike source. The simulation has shown that the expected signal would be a narrow spot of light in the direction of the center of the Sun, and allowed an evaluation of the fraction of decays yielding visible photons as function of the chosen neutrino ν_1 mass, m_1 , and Δm^2 values. The lower limits obtained from the 1999 TSE range between $1.8 \times 10^{-2} \text{ s eV}^{-1} < \tau_0/m < 14.5 \text{ s eV}^{-1}$.

It may be worth to mention that the Particle Data Group best fit lower limit for the neutrino lifetime, in the printed version of 2002 was $7 \times 10^9 \text{ s eV}^{-1}$, while in the 2003 partial upgrade the best fit is only 300 s eV^{-1} [6].

In this paper we present the results obtained from the analysis of our 2001 TSE observations. This experiment allowed the collection of better resolution data, so the real spatial distribution of the solar neutrino yield had to be considered. The recent SNO results [9,10] favor the LMA solution and indicate also the presence of a ν_τ component in the solar neutrino flux at the Earth level. Furthermore, they indicate a possible lower limit for the sum of the neutrino masses of about $4.8 \times 10^{-2} \text{ eV}$. The WMAP (Wilkinson Microwave Anisotropy Probe) results after the first year flight, assuming three degenerate neutrino species [21] limit the mass of the neutrino to $\leq 0.23 \text{ eV}$ (95% CL).

The new Monte Carlo simulation code developed for the analysis of our 2001 data was described elsewhere [22]. It is based on the latest updates of the Standard Solar Model [23] and on a full 3-D geometry of the solar neutrino production, decay and photon detection, as initially proposed in [24].

2 Experimental data

The experimental data used for this search consist of two sets of digital images, obtained with two different instruments and different exposures, magnifications and resolutions, during the TSE of June 21st 2001. For the observation we have chosen a location 50 km North of Lusaka, Zambia, in the vicinity of a farm that could provide electrical power. The site was located at 14°56' lat. S, 28°14' long. E, and at an altitude of about 1200 m a.s.l. The distance to the centrality line was approximately 8 km.

One data set (referred to as “set A”) consists in 4149 frames obtained from a digital film made with a video-camera equipped with a 2× telelens and a 10× optical zoom. The recording rate was 25 frames per second. The field of view of each pixel of the CCD camera was 9.97” × 10.74” (arcsec).

The second data set (that will be referred to as “set B”) consists in 10 digital photographs made with a Matsukov - Cassegrain telescope (90 mm ϕ and $f = 1250$ mm), coupled to a digital camera. The camera was set to emulate a photographic film of 400 ASA sensitivity. The exposure time for each image was 2 s, and the digital camera automatically adjusted the aperture as function of the luminosity of the solar corona. We took into consideration this effect in our analysis. In order to avoid systematic effects due to the optical system or to the CCD, we slightly changed the orientation of the telescope from one frame to another. The field of view of each pixel of the CCD was 1.14” × 1.14”.

For both data sets and for each image, we determined the center of the dark disk of the Moon. The signal of a possible radiative decay of solar neutrinos during their flight from the Moon to the Earth should be correlated to the position of the center of the Sun. The totality phase of the TSE at the observation point lasted about $t_{tot.} = 3.5$ minutes, so the center of the Sun continuously changed its position with respect to the center of the dark disk of the Moon. In equatorial coordinates, the velocity components (declination and ascension) of the relative movement of the Moon center with respect to the Sun center were: $v_\delta \simeq 0.055''/s$ and $v_\alpha \simeq 0.758''/s$. As the angle between the “horizontal” x-axis of our images and the ecliptic was about 53^0 , we computed the “x” and “y” components of the relative velocity of the center of the Moon with respect to the Sun center: $v_x \simeq 0.455''/s$ and $v_y \simeq 0.033''/s$. The distance (in arcsec) between the two centers was computed for any time t from the start of the totality, knowing that at $t = t_{tot.}/2$ the Moon and the Sun centers were coincident. This allowed us to know, for each image, the shift (in pixels) between the Moon center and the center of the Sun, and thus the displacement to apply to the images before adding one to another.

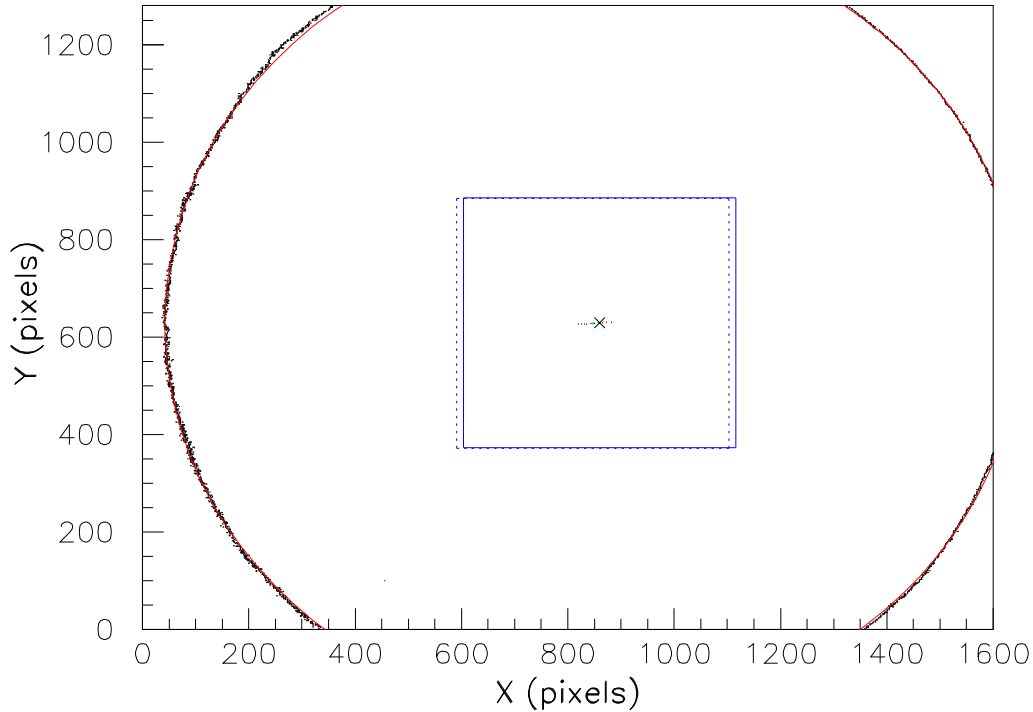


Fig. 1. Illustration of the procedure used to select the largest dyadic square centered on the center of the Sun from the pictures of set B obtained during the TSE. See text for details.

The procedure to search for possible signals in each data set is based on the wavelet decomposition of each of the two total images, and we retained as useful data only the larger dyadic squares around the center of the Sun. In the case of set A, the dimension of this square is 64×64 pixels², while for set B is 512×512 pixels². Fig. 1 illustrates this procedure for a typical image of data set B. The border of the dark Moon disk is obtained by requiring a variation of 100 Aquisition Digital Units (ADU) from a pixel to the next one. The resulting shape is then fit to a circle. The border pixels and the fit circle are shown in Fig. 1. The position of the center of the Sun with respect to the center of the Moon is calculated as a function of the time at which the photo was made; it is represented in Fig. 1 by the small cross in the middle of the image. The 512×512 pixels² area, centered on the center of the Sun, is then obtained for each picture (the solid rectangle in Fig. 1); all the similar zones of the 10 pictures are summed together for further processing. The relative displacement of the Sun center from the beginning to the end of data taking is indicated in Fig. 1 by the small points at the center of the field; a 512×512 pixels² rectangle centered on the center of the Moon is also drawn (the dotted square). This procedure was applied to all digital video frames of data set A and to all digital photographs of data set B; the sums were then computed

for each color channel (red, green and blue) and for their sum (the “white” channel).

3 Data analysis

The MC simulations of the solar neutrino radiative decays [22], $\nu_2 \rightarrow \nu_1 + \gamma$, assuming $\Delta m_{21}^2 = 6 \times 10^{-5} \text{ eV}^2$, $10^{-3} \leq m_1 \leq 3 \times 10^{-1} \text{ eV}$, indicate that the expected signal in the optical band should consist in a narrow luminosity peak (about 50” wide) in the direction of the center of the Sun. If the ν_3 mass eigenstate is also present in the solar neutrino flux at the Earth, the $\nu_3 \rightarrow \nu_{2,1} + \gamma$ decays, with $\Delta m_{32(1)}^2 = 2.5 \times 10^{-3} \text{ eV}^2$, would yield a broader signal (about 250”), possibly showing some “rings” at 200 - 300 arcseconds, concentric to the position of the center of the Sun. Most of the background light (diffraction of the coronal light on the borders of the Moon, diffuse sky light, ashen light (light reflected by the Earth on the surface of the Moon), etc.), are characterized by larger angular scales. Thus the wavelet decomposition of the compound images is a proper tool to search for a possible decay signal.

We used the simple Haar wavelet basis [25]. The n -order term of the decomposition is obtained by dividing the $N \times N$ pixels² image in square fields of $N/2^n \times N/2^n$ pixels² and averaging the luminosity in each field; the averages are then removed and the resulting image, the n -order residual, can be used to obtain the $(n + 1)$ -order term. Thus, each decomposition term results in an image in which objects of the corresponding scale are dominant, while the residuals contain information for smaller dimension scales.

The decay signal is searched for by averaging the luminosity of the images over “rings” centered on the position of the center of the Sun. As the wavelet analysis requires a dyadic dimension of the field (the number of pixels on each border of the image is a power of 2), there is no “central pixel”; so we have considered each of the four pixels adjacent to the image center as “central” and then averaged the obtained luminosity profiles.

Fig. 2 shows the luminosity profiles obtained from the total images A (Fig. 2a) and B (Fig. 2b). Both graphs refer to the “white” channels, that is the sum over the three color channels. The vertical scales are expressed in ADU; the meaning of 1 ADU (different for each instrument) is discussed in Section 4. The difference between the two total images is due to the different CCD sensitivities, spatial resolution and optical features of the instruments. Data set A presents no clear structure, data B might contain some at relatively large θ .

Most of the background is removed by the wavelet decomposition. Fig. 3 shows

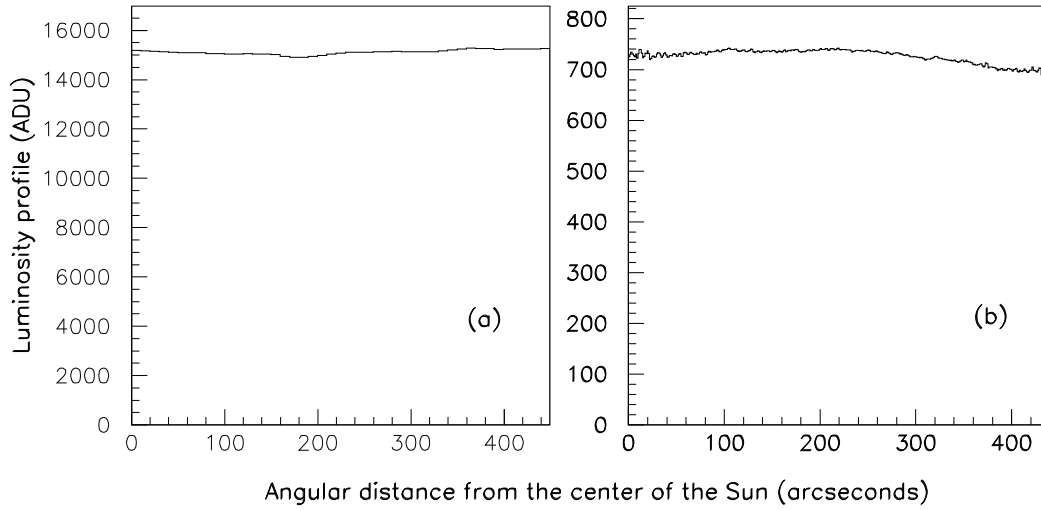


Fig. 2. Luminosity profiles (in white light) for (a) the compound image A and (b) B (raw data).

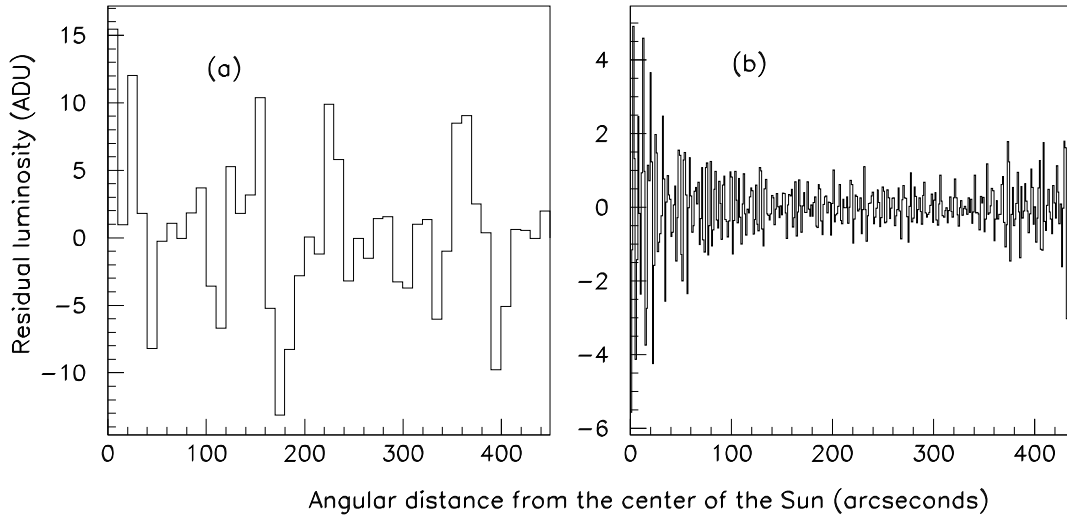


Fig. 3. Luminosity profiles of the last residuals from the wavelet decomposition of (a) the compound images A -fifth order-, and (b) B -eight order-. Both profiles are obtained in the “white” channel.

the residuals of order 5 for the data A, and of order 8 for the B data, in the “white” channel. In these residuals (the highest possible order for each data sets), the contributions of structures larger than 2×2 pixels² are removed. Both Figs. 3a and 3b are dominated by fluctuations, so we may conclude that at our experimental sensitivities, data sets A and B do not contain indication for a narrow light excess from the direction of the center of the Sun. The increase of the fluctuation amplitudes near the limits of the angular range, clearly noticeable in Fig. 3b, is natural, as the number of pixels that contribute to

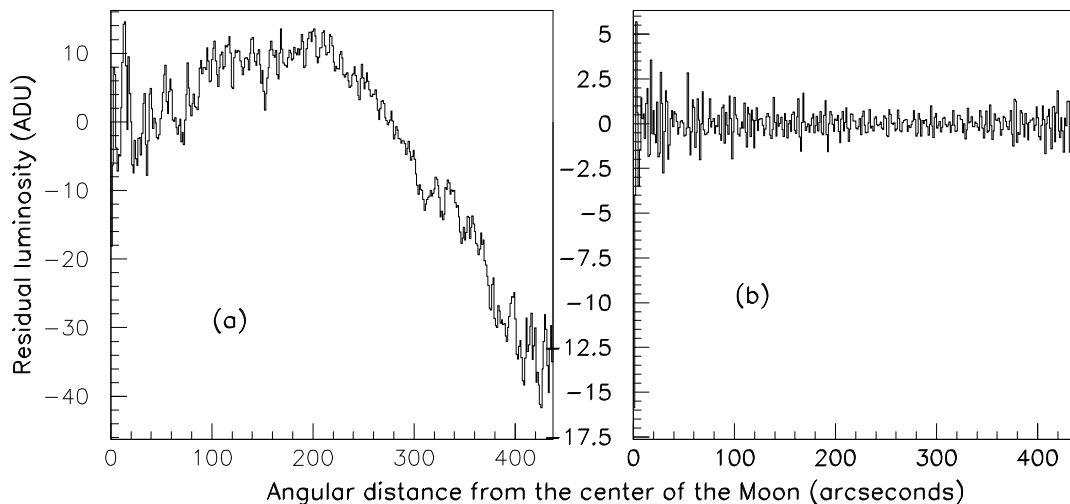


Fig. 4. “White” light luminosity profiles obtained by aligning the images of data set B with respect to the center of the Moon, from (a) the 0 order (thus after removing the average luminosity) and (b) the 8th order residuals

the average luminosity in that regions is smaller than in the rest of the image.

We recall that maxima confined to the first bin and present in all color channels were observed in the TSE 1999 data [17,18,19]. Probably we observed the so-called “Poisson spot” consisting in a peculiar diffraction phenomenon that is produced when a circular opaque object, with size much smaller than the distance to a screen, but much larger than the light wavelength, is illuminated by a parallel beam [26]. In such conditions, a point-like spot of light could be observed on the screen, in the middle of the shadow of the object. In 1999 we analyzed a video filmed close to the point of maximum eclipse, when the center of the Sun, the center of the Moon and the observer were in very good alignment.

Since in 2001 we were in a location 8 km away from the line of centrality of the TSE, one does not expect that the same effect is seen. Such signal could be enhanced by aligning the 10 pictures with respect to the center of the Moon. Fig. 4 shows the results of such an analysis. In Figs. 4a and 4b there is no peak associated with the center of the Moon disk. A darker spot is instead seen in the center of the Moon; it should correspond to the dark Schröter area. The structures in Fig 4a may be produced by the image of the Moon surface in the light of the Sun reflected by the Earth. Their absence in Fig. 4b is due to the rejection of large structures by the wavelet decomposition.

The expected signal from a decay (1), considering its MC estimated width [22], should be better seen in the fourth order wavelet term of data sets A and B, as it corresponds to structures with about 40” - 60” width. Fig. 5 shows

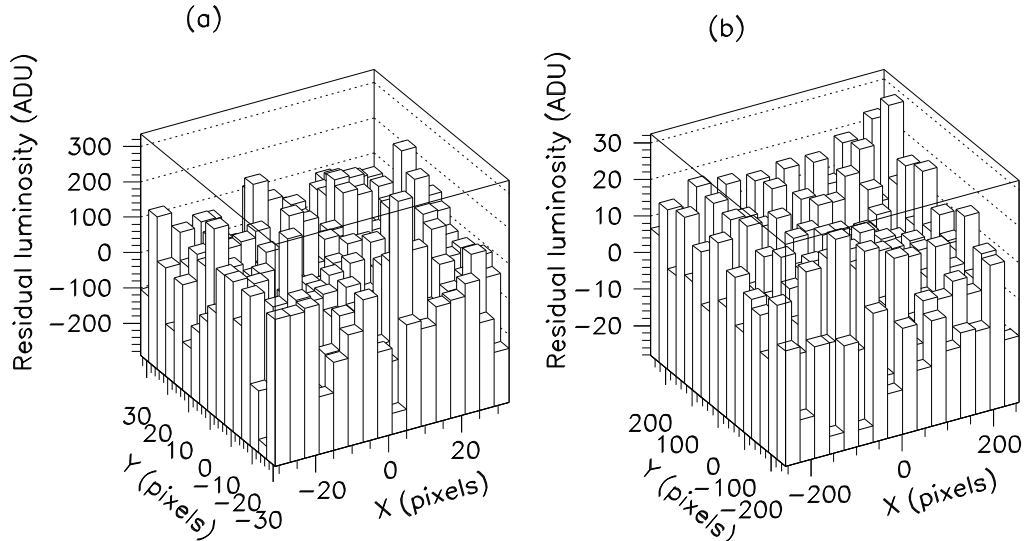


Fig. 5. “White” light luminosity distributions of the fourth order wavelet term of (a) the summed images A and (b) B (centered on the Sun).

the luminosity distributions for this term. Note that each bin is an average over 4×4 pixels in the case of data set A (Fig. 5a), and over 32×32 pixels for set B (Fig. 5b). No central maximum is present in both data sets, and we can use these wavelet terms to determine lower lifetime limits for the investigated decay.

The search for the $\nu_3 \rightarrow \nu_{2,1} + \gamma$ decay is more difficult, as the expected signal is broader (about $200'' - 300''$) [22]. Since the wavelet decomposition could remove broad signals, we searched for the corresponding signal in the raw data. Data set A does not exhibit such a signal (Fig. 2a), but the luminosity curve obtained from set B (Fig. 2b) could suggest the presence of the expected signal. Considering the good resolution and sensitivity of instrument B, we assumed that the ashen light (the luminosity of the Moon surface due to the light of the Sun reflected by the Earth) could be responsible for most of the signal seen in B. In order to verify that, we performed the same analysis on an image of the full Moon, obtained with the same telescope and camera. The results of this test are shown in Figs. 6a and 6b. The structures in Fig. 6a are similar to those in Figs. 2b and 4a; we should take into consideration that the Earth reflects the light of the Sun as a convex mirror, thus the central part of the Moon receives more light from the Earth than the rest of it. Instead the Sun illuminates the Moon uniformly. This observation suggests that we cannot simply remove the image of the full Moon from the data, as it would create a fake signal in the central part of the resulting image. Thus, one should develop a reliable model of the ashen light; alternatively one should use the wavelet

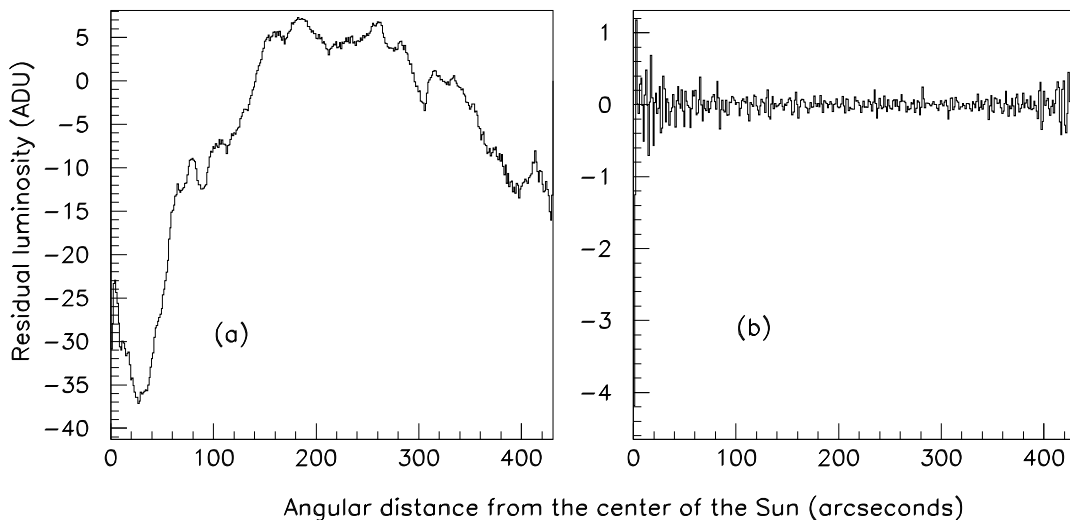


Fig. 6. “White” light luminosity profiles obtained from an image of the full Moon from (a) the 0 order and (b) the 8th order residuals. The Moon image was obtained with the same equipment used for taking the set B data.

decomposition. Note that the exposure conditions for the image of the full Moon were different than those during the eclipse, so the ADU values are not directly comparable. As we cannot determine which is the real contribution of the ashen light in set B, we can use the results only to determine a lower limit for the ν_3 lifetime.

4 Calibrations

The luminosity values given in the previous Sections in ADU have to be converted in numbers of photons hitting each pixel of the CCD’s of our detectors. For this purpose two sets of calibrations were made, using the monochromators of the Catania and Bologna Astronomical Observatories. The obtained calibration curves are consistent one with the other. We took care to calibrate the instruments in conditions as close as possible to the conditions in which the TSE data were recorded. The digital videocamera was operated in the same conditions as during the eclipse; the pictures with the digital camera were taken with exposures of 2 s, and a fixed diaphragm aperture (f/2.5). As mentioned in Section 2, the 10 digital pictures in data set B were obtained with different apertures; the total 20 s of exposure in the eclipse conditions is equivalent to about 4.7 s in the calibration conditions.

Fig. 7 shows the calibration curves obtained. In the vertical scales are indicated the number of incident photons that produce 1 ADU in one pixel of the CCD’s. Each curve corresponds to one color channel. From these calibrations it follows

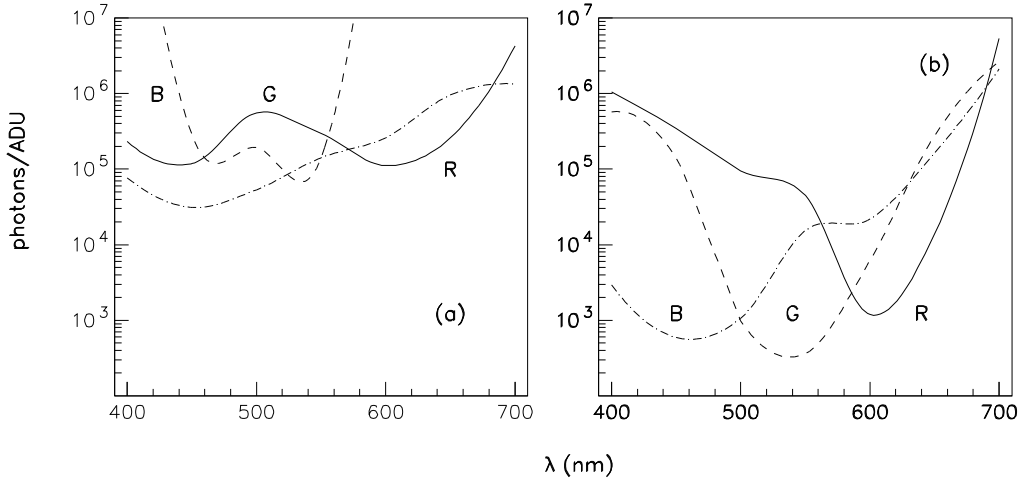


Fig. 7. Calibration curves (number of incident photons that produce one ADU plotted as function of the wavelength): (a) for the digital videocamera, and (b) the digital camera with telescope. The results concerning the Red, Green and Blue channels are represented as solid, dashed and dot-dashed curves, respectively.

that the wavelength averaged number of visible photons that produces one ADU in the “white” channel of data set A is about 7.3×10^4 , while for data set B is two orders of magnitude smaller: 8.9×10^2 . This could explain why we may see the ashen light only in data B.

5 Results and discussions

Both data A and B were processed in order to search for signals produced by a possible radiative decay of the heavier component of solar neutrinos. In the absence of a valid signal, we used the two sets to obtain lower limits for the neutrino radiative decay lifetime.

Let us assume the simplest scenario in which the Sun electron neutrinos are a superposition of only two mass eigenstates ν_1 , ν_2 , with a mixing angle θ_{12}

$$|\nu_e\rangle = |\nu_1\rangle \cos \theta_{12} + |\nu_2\rangle \sin \theta_{12}, \quad (2)$$

Using the calibrations of our instruments, we transform the ADU into numbers of photons N_γ , that produced the analyzed images. The lifetimes of the $\nu_2 \rightarrow \nu_1 + \gamma$ decay in the laboratory frame of reference, can be calculated from the

standard deviations of the fourth order terms of the wavelet decomposition of our data

$$N_\gamma = P\Phi_2 S_M t_{obs} \left(1 - e^{-\frac{\langle t_{ME} \rangle}{\tau}}\right) e^{-\frac{t_{SM}}{\tau}}, \quad (3)$$

where P are the mass - dependent probabilities estimated by the MC simulation [22], $\Phi_2 = \Phi_\nu \sin^2 \theta_{12}$, (Φ_ν is the flux of solar neutrinos at the Earth (or Moon) and θ_{12} the mixing angle) is the local flux of solar ν_2 mass eigenstate neutrinos, S_M is the area of the Moon surface covered by the analysis (the area of the square on the Moon that is visualized inside the dyadic square) and t_{obs} is the time of observation. $\langle t_{ME} \rangle$ is the average time spent by solar neutrinos inside the observation cone (about one third of the flight time from the Moon to the Earth), and t_{SM} is the time of flight of the neutrinos from the Sun to the Moon [22].

The MC probabilities P are shown in Figs. 8a,b, for data sets A and B, respectively. Assuming that a neutrino decay occurs during the flight of solar neutrinos between the Moon and the Earth, inside the region of space “visible” by the experiment, and that the emitted photon reaches the detector, the probability P includes kinematic effects (dominated by the assumed polarization α of the ν_2 beam), the request that the emitted photon should be in the visible energy range and the “imprints” of the initial neutrino characteristics (energy and “birth” position), according to the SSM [23]. The simulations were made for three possible values of the polarization of the decaying neutrinos: $\alpha = -1$, which corresponds to Dirac left-handed neutrinos (like for the massless neutrinos in the Standard Model), $\alpha = 0$ (Majorana neutrinos), and for right handed Dirac neutrinos ($\alpha = +1$).

Similar simulations were made assuming $\nu_3 \rightarrow \nu_{(2,1)} + \gamma$, with $\Delta m_{3,(2,1)}^2 = 2.5 \times 10^{-3} \text{ eV}^2$. The computed probabilities are presented in Fig. 9.

The 95% CL lower limits for the ν_2 lifetime, in our case of no signal, are obtained by the substituting in Eq. 3 N_γ with $3\sigma_{N_\gamma}$ of the fourth order wavelet terms decomposition of the data. They are shown with thicker lines in Figs. 10a (data A) and 10b (data B), assuming that ν_2 is a Dirac (lefthanded or righthanded) or a Majorana neutrino.

The recent limits obtained from the Borexino Counting Test Facility [14] are also shown, for comparison. The arrows labelled “SNO” and “WMAP” indicate the lower neutrino mass limit reported by SNO [9,10], and the upper mass limit obtained by WMAP [21]. The limit obtained by the first TSE experiment [15] is indicated by the horizontal arrow; note that this limit, obtained using different physical hypotheses, is valid for neutrino masses of few eV.

Neutrino lifetime values larger than our lower limits are not in conflict with

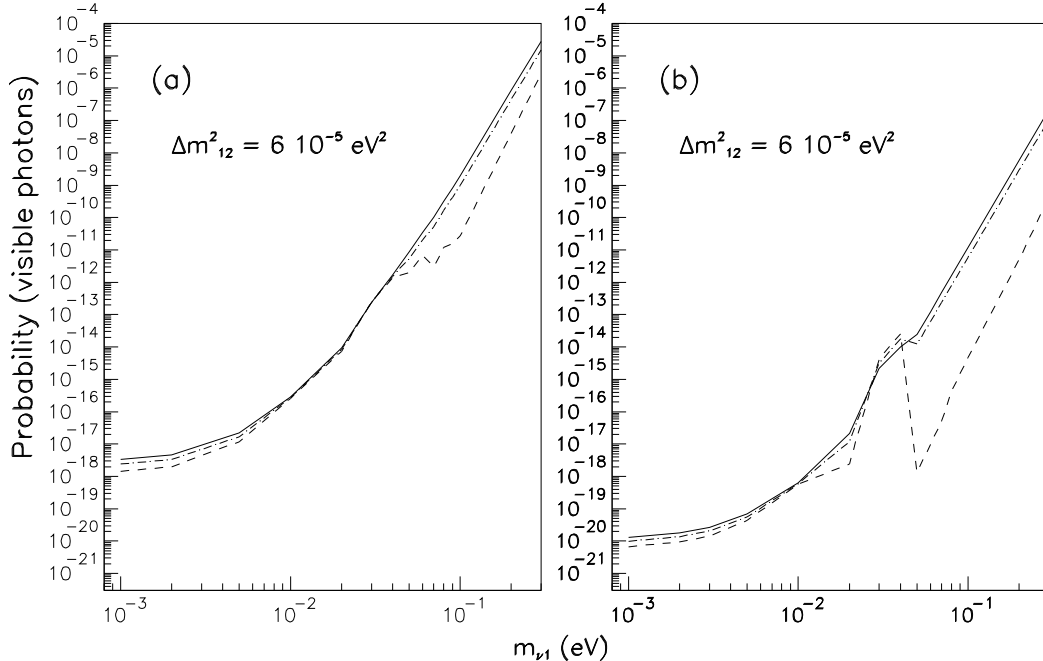


Fig. 8. Monte Carlo Probabilities for the production and arrival to the detector of the decay photons resulting from $\nu_2 \rightarrow \nu_1 + \gamma$ transitions during the neutrino flight from the Moon to the Earth. The simulations were made for (a) data set A and (b) set B. The solid, dot-dashed and dashed lines correspond to three different neutrino polarizations, $\alpha = -1, 0$ and $+1$, respectively.

the oscillation explanation of the solar neutrino deficit. The neutrino time of flight from the Sun to the Earth is about 500 s (in the laboratory frame of reference). The Lorentz boost for a solar neutrino with a mass of about 0.02 eV is $\gamma \simeq 1.5 \times 10^7$, so the fraction of ν_2 that would decay into $\nu_1 + \gamma$, assuming $\tau_0 \simeq 60$ s (in the c.m.) would be only $\simeq 5 \times 10^{-7}$.

The atmospheric neutrino data indicate $\nu_\mu \rightarrow \nu_\tau$ oscillations with maximal mixing [31,32,33]. The two generation mixing of solar neutrinos is an approximation; the “heavy” component of the flux could then be a mixture of ν_2 and ν_3 mass eigenstates. The mixing angle θ_{13} is not yet measured, but it should be small; we assume $\sin^2 \theta_{13} \simeq 0.1$. Data set A does not contain “signals” similar to the MC expectations [22], and in data set “B” the presence of the ashen light creates a luminosity profile that could mask a possible signal. In both cases, we obtain the 95% CL ν_3 lifetime lower limits, from the raw images, shown in Fig. 11.

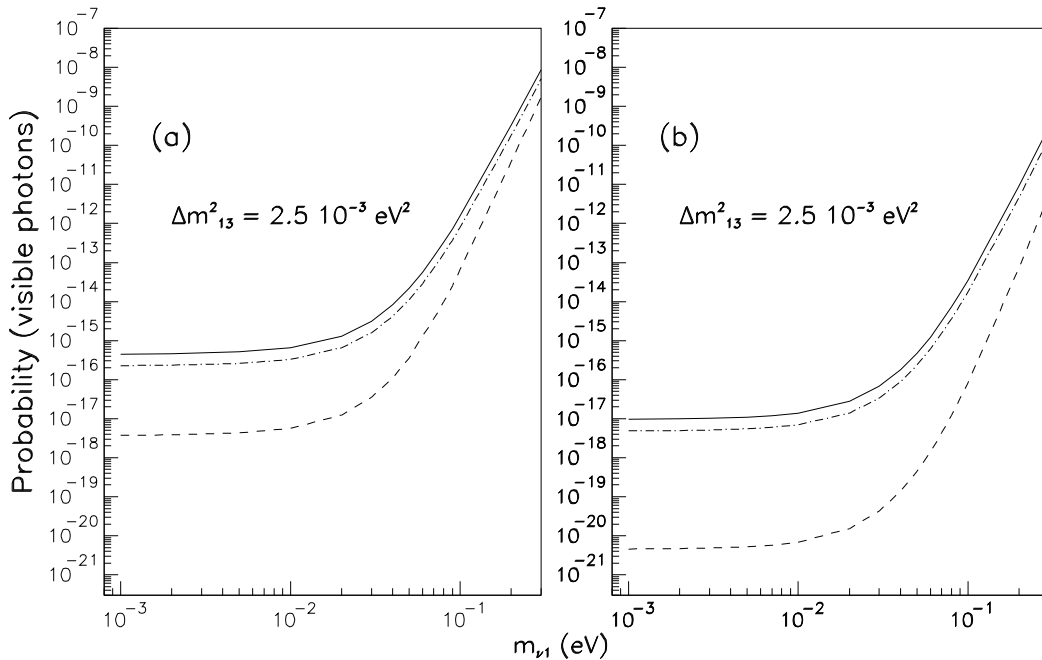


Fig. 9. Monte Carlo Probabilities for the production and arrival to the detector of the decay photons resulting from $\nu_3 \rightarrow \nu_{(2,1)} + \gamma$ transitions during the neutrino flight from the Moon to the Earth. The simulations were made in the conditions of (a) data set A and (b) set B. The solid, dot-dashed and dashed lines correspond to three different neutrino polarizations, $\alpha = -1, 0$ and $+1$, respectively.

6 Conclusions

We analyzed two sets of digital images obtained during the June 21st 2001 total solar eclipse, in Zambia, looking for possible radiative decays of solar neutrinos, yielding visible photons.

Data set A consists in a large number of frames recorded with a digital video-camera; it has a relatively large integration time, but a modest space resolution.

Set B consists of 10 pictures taken with a digital camera coupled to a small telescope. Its time coverage is poorer than for set A, but it has a better space resolution and the instrument sensitivity was an order of magnitude better.

The proper lower lifetime limits (95% CL) obtained for the $\nu_2 \rightarrow \nu_1 + \gamma$ decays of lefthanded neutrinos range from $\tau_0/m_2 \simeq 10 \text{ s eV}^{-1}$ to $\simeq 10^9 \text{ s eV}^{-1}$, for $10^{-3} \text{ eV} < m_{\nu_1} < 0.1 \text{ eV}$, see Fig. 10. These limits are among the best obtained from direct measurements, demonstrating the potentiality of neutrino decay experiments during total solar eclipses (or possibly made in space, using the

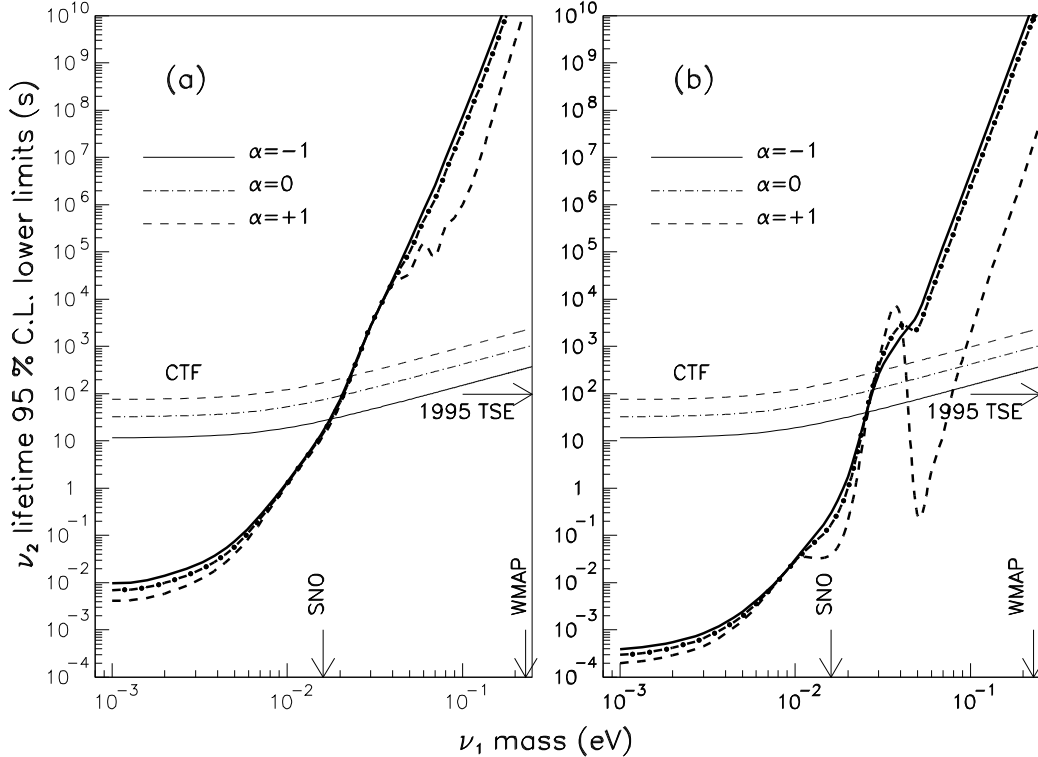


Fig. 10. The 95% CL lower limits for the ν_2 proper lifetime, as function of the m_{ν_1} , obtained from data sets (a) A and (b) B. The results are valid in a neutrino mixing scenario with only two generations, and $\Delta m_{2,1}^2 = 6 \times 10^{-5} \text{ eV}^2$. The discontinuities in the proper lifetime limits for righthanded neutrinos originate in the MC probabilities and reflect the changes in the initial neutrino energy imposed by the condition of obtaining visible decay photons pointing to the Earth. Other relevant limits are also indicated (see text).

Earth as light absorber [24]). The lab. lifetime limits are about 10^7 times larger, thus the fraction of neutrino decays from the Sun to the Earth would be negligible.

A similar analysis was made for a possible $\nu_3 \rightarrow \nu_{2,1} + \gamma$ decay, assuming $\sin^2 \theta_{31} \simeq 0.1$ (the value of this mixing angle is not known). No signal compatible with a possible $\nu_3 \rightarrow \nu_{2,1} + \gamma$ is seen. The obtained 95% C.L. ν_3 proper lifetime lower limits, for $m_1 \geq 10^{-2} \text{ eV}$ and for $\alpha = -1, 0$, are about two orders of magnitude lower than for the ν_2 , Fig. 11.

New observations, in better technical conditions, during forthcoming TSE's should be considered.

An attempt along these lines was made during the December 2002 eclipse, but the weather conditions in South Africa did not allow any observation. We intended to use three portable telescopes, equipped with astronomy type CCD's. The sensitivity would have been about two orders of magnitude better

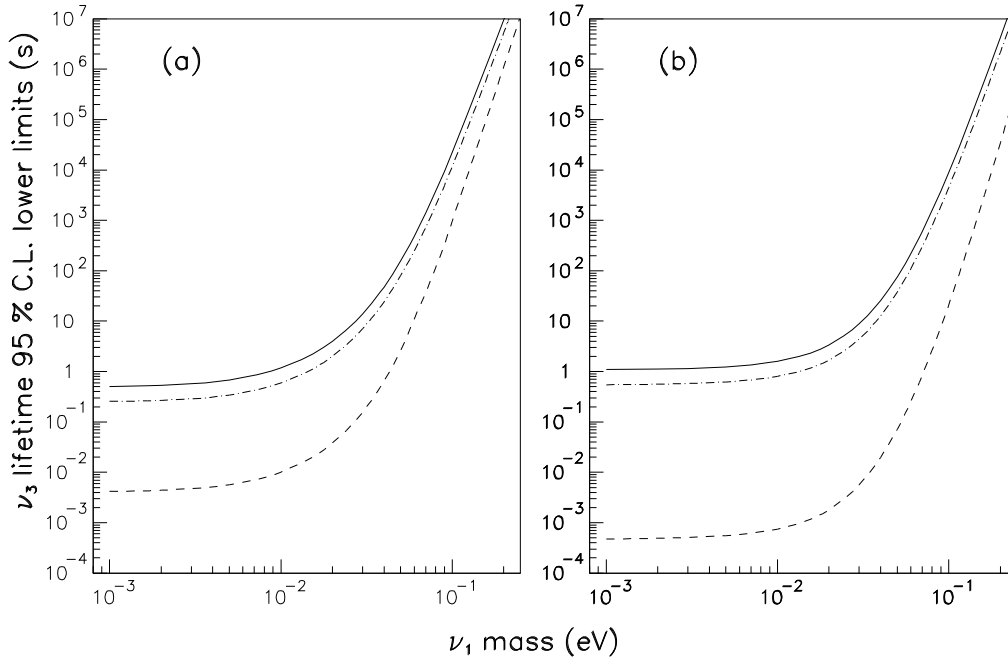


Fig. 11. The 95% CL lower limits for the ν_3 proper lifetime, as function of the ν_1 mass, obtained from (a) set A (a) and (b) B. The solid, dot-dashed and dashed lines correspond to three different neutrino polarizations, $\alpha = 1, 0$ and -1 , respectively. The results are obtained in a neutrino mixing scenario with three generations, $\Delta m_{2,1}^2 = 5 \times 10^{-5} \text{ eV}^2$ and $\Delta m_{3,(2,1)}^2 = 2.5 \times 10^{-3} \text{ eV}^2$.

than what reported in this paper.

7 Acknowledgments

We would like to acknowledge many colleagues for useful comments and discussions. We thank the people of the Catania and Bologna Astronomical Observatories for their assistance during calibrations. Warm thanks are due to the Kiboko Safari, Lilongwe, Malawi, for their assistance during the expedition in Zambia. This work was funded by NATO Grant PST.CLG.977691 and partially supported by the Italian Space Agency (ASI), INFN and the Romanian Space Agency (ROSA).

References

- [1] G. Giacomelli and M. Sioli, *Astroparticle Physics*, hep-ex/0211035
- [2] S. Pakvasa and J.W.F. Valle, *Neutrino Properties Before and After KamLAND*, hep-ph/0301061

- [3] A.L. Melott, D.W. Sciama, *Phys.Rev.Lett.* **46** (1981) 1369.
- [4] H.L. Shipman and R. Cowsik, *Ap. J.* **247** (1981) L111.
- [5] D.W. Sciama, *Nucl.Phys.Proc.Suppl.* **38** (1995) 320.
- [6] K. Hagiwara et al. (P.D.G.), *Phys. Rev.* **D66** (2002) 0100001 and 2003 partial update (URL: <http://pgd.lbl.gov>).
- [7] S.A. Bludman, *Phys. Rev.* **D45** (1992) 4720.
- [8] A. Acker and S. Pakvasa, *Phys. Lett.* **B320** (1994) 320.
- [9] Q.R. Ahmad et al. (SNO Coll.), *Phys. Rev. Lett.* **87** (2001) 071301.
- [10] Q.R. Ahmad et al. (SNO Coll.), *Phys. Rev. Lett.* **89** (2002) 011301.
- [11] A. Bandyopadhyay, S. Choubey and S. Goswami, *Phys. Lett.* **B555** (2003) 33.
- [12] A.S. Joshipura, E. Massó and S. Mohanty, *Phys. Rev* **D66** (2002) 113008.
- [13] J. Bouchez et al., *Phys. Lett.* **B207** (1988) 217.
- [14] A.V. Derbin and O.Ju. Smirnov, *JETP Letters* **76** (2002) 483.
- [15] C. Birnbaun et al., *Phys. Lett.* **B397** (1997) 143.
- [16] S. Cecchini et al., *Astrophys. and Space Sci.* **273** (2000) 35.
- [17] S. Cecchini et al., Limits on radiative decays of solar neutrinos from a measurement during a solar eclipse, hep-ex/0011048
- [18] V. Popa et al., *Astrophys. and Space Sci.* **282** (2002) 235.
- [19] G. Giacomelli and V. Popa, in: M. Baldo Ceolin (Edt.), *Neutrino Oscillations in Venice*, Edizioni Papergraf (2001) 321; hep-ex/0110013
- [20] J.N. Bahcall, Standard Solar Models, astro-ph/9808162
- [21] D.N. Spergel et al., *Ap.J.* **148** (2003) 175.
- [22] S. Cecchini et al., *Astropart. Phys.* (2003) -in print-; hep-ph/0309107.
- [23] J.N. Bahcall, M.H. Pinsonneault and S. Basu, *Ap. J.* **555** (2001) 990.
- [24] J.-M. Frère and D. Monderen, *Phys. Lett.* **B431** (1998) 368.
- [25] Y. Fujiwara and J. Soda, *Prog. Theor. Phys.* **95** (1996) 1059
- [26] P.M. Rinard, *Am. J. Phys* **44** (1976) 70.
- [27] B.W. Lee and R.E. Shrock, *Phys. Rev.* **D16** (1977) 1444.
- [28] S.T. Petkov, *Yad. Fiz.* **25** (1977) 641.
- [29] E. Sato and M. Kobayashi, *Prog. Theor. Phys.* **58** (1977) 1775.
- [30] M.A. Beg, W.J. Marciano and M. Ruderman, *Phys. Rev.* **D17** (1978) 1395.

- [31] M. Ambrosio et al., *Phys. Lett.* **B434** (1998) 451; **B517** (2001) 59; **B357** (1995) 481.
- [32] M. Ambrosio et al., *Phys. Lett.* **B566** (2003) 35; **B478** (2000) 5.
- [33] Y. Fukuda et al., *Phys. Rev. Lett.* **81** (1998) 1562.